We are IntechOpen,
the world's leading publisher of
Open Access books
Built by scientists, for scientists

6,900
Open access books available

186,000
International authors and editors

200M
Downloads

Our authors are among the

154
Countries delivered to

TOP 1%
most cited scientists

12.2%
Contributors from top 500 universities

CLARIVATE ANALYTICS

BOOK CITATION INDEX

INDEXED

WEB OF SCIENCE™

Selection of our books indexed in the Book Citation Index
in Web of Science™ Core Collection (BKCI)

Interested in publishing with us?
Contact book.department@intechopen.com

Nonlinear Compensation Using Multi-Subband Frequency-Shaped Digital Backpropagation

Ezra Ip[1] and Neng Bai[2]
[1]NEC Labs America, Princeton, NJ
[2]University of Central Florida, Orlando, FL
USA

1. Introduction

As dense wavelength-division multiplexed (DWDM) systems push towards ever higher spectral capacities, the nonlinear Shannon's limit is rapidly being approached (Essiambre et al., 2008). Much research has been devoted to nonlinear compensation (NLC) algorithms that can undo deterministic nonlinear impairments to increase nonlinear capacity. All NLC algorithms are ultimately based approximate solutions to the inverse nonlinear Schrödinger equation (NLSE) that describes signal propagation in fiber. In forward propagation, assuming the signal is sufficiently narrowband where the slowly varying envelope approximation holds, a signal evolves as a Manakov equation (Marcuse et al. 1997):

$$\frac{\partial \mathbf{u}}{\partial z} = \left(\hat{\mathbf{D}} + \hat{\mathbf{N}}\right)\mathbf{u} \, , \tag{1}$$

where $\mathbf{u}(z,t) = \left[u_x(z,t) \quad u_y(z,t) \right]^{\mathrm{T}}$ is the Jone's representation of the slowly-varying baseband electric field envelope, $u_x(z,t)$ and $u_y(z,t)$ are the two polarization components.

$\hat{\mathbf{D}} = -\frac{1}{2}\boldsymbol{\alpha} - \boldsymbol{\beta}_1 \frac{\partial}{\partial t} - j\boldsymbol{\beta}_2 \frac{1}{2!}\frac{\partial^2}{\partial t^2} + \boldsymbol{\beta}_3 \frac{1}{3!}\frac{\partial^3}{\partial t^3}$ and $\hat{\mathbf{N}} = j\frac{8}{9}\gamma|\mathbf{u}|^2$ are the linear and nonlinear operators, with $\boldsymbol{\alpha}$, $\boldsymbol{\beta}_1$, $\boldsymbol{\beta}_2$, and $\boldsymbol{\beta}_3$ being 2×2 matrices representing attenuation, polarization-mode dispersion, group velocity dispersion and dispersion slope of the fiber, and γ being the fiber's nonlinear parameter. In the absence of noise, the forward propagation equation in (1) can be inverted via (Li et al. 2008):

$$\frac{\partial \mathbf{u}}{\partial (-z)} = \left(\hat{\mathbf{D}} + \hat{\mathbf{N}}\right)\mathbf{u} \, . \tag{2}$$

This operation is analogous to passing the received signal through a fictitious channel where each element in the fictitious channel exactly inverts the real elements in the forward-propagating channel (Fig. 1). In the presence of optical noise arising from optical amplifiers, the inverse NLSE is inexact. As the behavior of the NLSE becomes chaotic at high power, relative signal distortion increases, causing the nonlinear Shannon's limit to arise. All
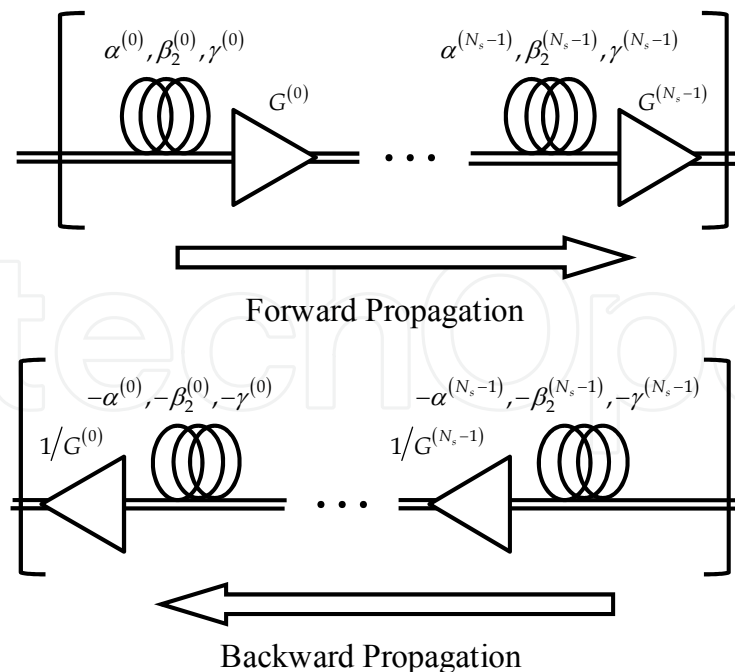
Fig. 1. Channel inversion via backpropagation.

nonlinear compensation (NLC) methods can be shown to be approximate solutions of the inverse NLSE.

The most advanced nonlinear compensation method is "digital backpropagation" (DBP), where the electric field $\mathbf{u}(z,t)$ is recovered by an optical-to-electrical downconverter and then sampled at the Nyquist rate (Ip & Kahn, 2010). The channel impairments are then inverted by numerically solving (2), usually via the split-step Fourier method (SSFM). The SSFM is an iterative algorithm that divides the fiber channel into small steps and then successively passing the signal through the linear and nonlinear operators at each step. For the SSFM algorithm to be accurate, the step size has to be small enough so that the phase rotation in time due to application of $\hat{\mathbf{N}}$ and the phase rotation in frequency due to application of $\hat{\mathbf{D}}$ are both sufficiently small. The step size requirement has been studied in (Sinkin et al. 2003, Zhang & Hayee 2008).

To date, digital backpropagation has not been demonstrated in real-time due to its high algorithmic complexity. Much recent research effort has focused on finding approximate algorithms that can approach DBP in performance, but has significantly lower algorithmic complexity. Some promising results have recently been reported, such as by lowpass filtering the nonlinear operator (Du & Lowery, 2010, Li, et al. 2011). In comparison with the traditional SSFM, which is "frequency-flat," filtered backpropagation exploits chromatic dispersion in fiber that causes different frequency components of a signal to propagate at different speeds. From the point of view of a given frequency component within a signal, the other frequency components "walkoff," causing an averaging effect on their resulting nonlinear interaction thus reducing the variance of their nonlinear distortion. As walkoff increases with frequency separation, the frequencies that lie closest to the frequency component of interest will contribute greater nonlinear distortion than those frequencies that are far away. This effect can be fully exploited by using pre- and post-filters in the calculation of the nonlinear operator.

We will explore an enhanced DBP algorithm, where the nonlinear perturbation $\hat{\mathbf{N}} \cdot \mathbf{u}$ at each step is computed via multiple subbands: for each subband, different pre- and post-filters are used. Although the complexity required to compute $\hat{\mathbf{N}} \cdot \mathbf{u}$ is increased, the greater accuracy of the estimate enables larger step sizes. Furthermore, performance can be traded off against complexity by varying either the number of steps or number of subbands.

The outline of this chapter will be as follows. In Section 2, the theory of filtered DBP will be introduced from the point of view of casting the NLSE as a third-order Volterra series. The equations for computing pre-filter will be derived. In Section 3, the DSP architecture needed to implement filtered DBP will be given, and we will revisit the physical intuition for FS-BP. Simulation results will be presented in Section 4.

2. Theory

2.1 Single-polarization

2.1.1 Volterra series model

We begin by considering the NLSE for a single-polarization signal. Let $u(z,t)$ be the scalar electric field in the signal polarization of interest. Ignoring pulse polarization-mode dispersion (PMD) in fiber, the inverse scalar NLSE is given by (Agrawal, 2001):

$$\frac{\partial u}{\partial(-z)} = -\frac{\alpha}{2}u - j\frac{\beta_2}{2}\frac{\partial^2 u}{\partial t^2} + j\gamma|u|^2 u \tag{3}$$

Resolving $u(z,t) \sim \sum_k u_k(z)e^{j\omega_k t}$ in terms of its spectral components $u_k(z)$, where the frequencies are evenly spaced $\omega_k = k\Delta\omega$, we obtain a set of coupled equations:

$$\frac{du_k}{d(-z)} = \left(-\frac{\alpha}{2} + j\frac{\beta_2\omega_k^2}{2}\right)u_k + j\gamma\sum_{\substack{j,l,m \\ \in S[k]}} u_j u_l u_m^* \; . \tag{4}$$

In the absence of nonlinearity ($\gamma = 0$), the right-hand side of (4) gives the chromatic dispersion compensation filter as $H^-(\omega_k) = \int_0^L \frac{\alpha(z)}{2} - j\frac{\beta_2(z)}{2}\omega_k^2 \, dz$. When $\gamma \neq 0$, the set $S[k] \in \{j,l,m : j+l-m = k\}$ denote the frequencies that interact through the Kerr nonlinearity to produce a polarization at ω_k. The term for which $j = m = k$ denotes intra-channel self-phase modulation (ISPM); the terms for which $j = m \neq k$ denotes intra-channel cross-phase modulation (IXPM); while the remaining terms are intra-channel four-wave mixing (IFWM). Using a third-order perturbation technique developed by (Nazarathy 2008), the signal can be expanded as $u_k(z) = u_k^{(1)}(z) + u_k^{(3)}(z)$, where the first- and third-order terms satisfy:

$$\frac{du_k^{(1)}}{d(-z)} = \left(-\frac{\alpha}{2} + j\frac{\beta_2\omega_k^2}{2}\right)u_k^{(1)} \text{, and} \tag{5}$$

$$\frac{du_k^{(3)}}{d(-z)} = \left(-\frac{\alpha}{2} + j\frac{\beta_2\omega_k^2}{2}\right)u_k^{(3)} + j\gamma\sum_{\substack{j,l,m\\ \in S[k]}} u_j^{(1)}u_l^{(1)}u_m^{(1)*}.$$ (6)

Let $v_k(z) = u_k(z)\exp\left(\int_z^L -\left(\frac{\alpha(z')}{2} - j\frac{\beta_2(z')\omega_k^2}{2}\right)dz'\right)$ be a distanced-normalized spectral

components of the signal, where L is the step size. We can similarly decompose $v_k(z)$ as

$v_k(z) = v_k^{(1)}(z) + v_k^{(3)}(z)$, from which:

$$\frac{dv_k^{(1)}}{d(-z)} = 0 \text{, and}$$ (7)

$$\frac{dv_k^{(3)}}{d(-z)} = j\sum_{\substack{j,l,m\\ \in S[k]}} v_j^{(1)}v_l^{(1)}\left(v_m^{(1)}\right)^* \times \gamma(z)\exp\left(\int_z^L \alpha(z') + j\Delta\beta_{jlm}(z')dz'\right).$$ (8)

where $\Delta\beta_{jlm}(z) = \beta_2(z)\Delta\omega^2(l-k)(j-k)$.

We first assume the fiber parameters remain constant throughout this step, and there are no optical amplifiers in between. The nonlinear perturbation is then given by a third-order Volterra series:

$$v_k^{(3)}(0) = -j\sum_{\substack{j,l,m\\ \in S[k]}} D_{jlm}^{FWM} v_j^{(1)}v_l^{(1)}\left(v_m^{(1)}\right)^*,$$ (9)

where,

$$D_{jlm}^{FWM} = \gamma\exp\left(\left(\alpha + j\Delta\beta_{jlm}\right)L\right)\cdot\frac{1-\exp\left(-\left(\alpha + j\Delta\beta_{jlm}\right)L\right)}{\alpha + j\Delta\beta_{jlm}},$$ (10)

We can define $L_{jlm}^{FWM} = \dfrac{1-\exp\left(-\left(\alpha + j\Delta\beta_{jlm}\right)L\right)}{\alpha + j\Delta\beta_{jlm}}$ to be the "effective length" of the FWM

process involving frequencies ω_j, ω_l and ω_m. We then have $D_{jlm}^{FWM} = \gamma e^{\left(\alpha + j\Delta\beta_{jlm}\right)L}\cdot L_{jlm}^{FWM}$.

Clearly, as $|l-k|$ and $|j-k|$ increases (i.e., frequencies far from ω_k), $\Delta\beta_{jlm}$ increases, and

hence the strength of their nonlinear coupling on ω_k (i.e., D_{jlm}^{FWM}) decreases.

More generally, we can also consider that in the integration from $z = L$ to $z = 0$, there are

N_s spans of fiber, with an optical amplifier after each span (Fig. 2). Let $\alpha^{(n)}$, $\beta_2^{(n)}$ and $L_f^{(n)}$

be the attenuation, dispersion and length of the n-th fiber, and let $G^{(n)}$ be the gain of the n-th amplifier. Carrying out the integration inside the exponent in (8) we get:

$$\frac{dv_k^{(3)}}{d(-z)} = j \sum_{\substack{j,l,m \\ \in S[k]}} v_j^{(1)} v_l^{(1)} \left(v_m^{(1)}\right)^* \times \frac{\gamma^{(n)}}{G^{(n)}} \exp\left(\left(\alpha^{(n)} + j\Delta\beta_{jlm}^{(n)}\right)(z_n - z)\right) \times$$

$$\left[\prod_{n'=n+1}^{N_s-1} \frac{1}{G^{(n')}} \exp\left(\left(\alpha^{(n')} + j\Delta\beta_{jlm}^{(n')}\right)L_f^{(n')}\right)\right] \tag{11}$$
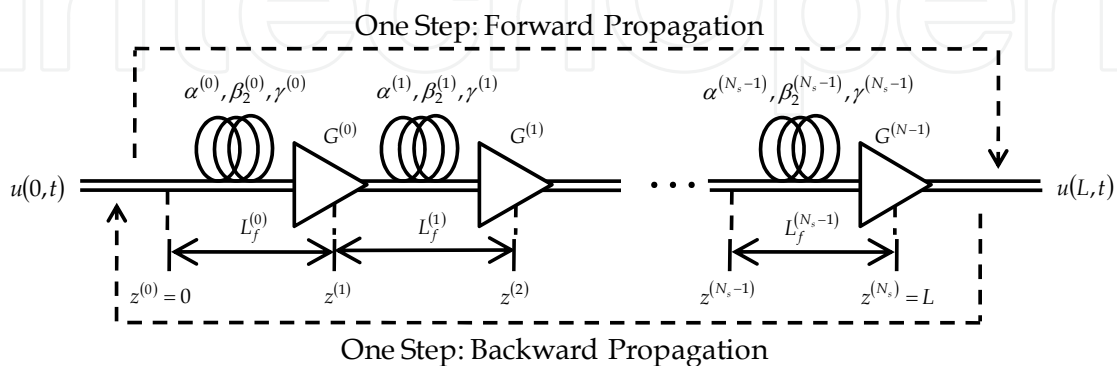
for $z_{n-1} \le z < z_n$.

Fig. 2. Solving the NLSE with step size equal to N_s heterogeneous spans of fiber.

At the output of the step, the perturbation term have a third-order Volterra series:

$$v_k^{(3)}(0) = -j \sum_{\substack{j,l,m \\ \in S[k]}} D_{jlm}^{FWM} v_j^{(1)} v_l^{(1)} \left(v_m^{(1)}\right)^*, \tag{12}$$

where

$$D_{jlm}^{FWM} = \sum_{n=0}^{N_s-1} \frac{\gamma^{(n)}}{G^{(n)}} \exp\left(\left(\alpha^{(n)} + j\Delta\beta_{jlm}^{(n)}\right)L_f^{(n)}\right) L_{jlm}^{FWM(n)} \times$$

$$\left[\prod_{n'=n+1}^{N_s-1} \frac{1}{G^{(n')}} \exp\left(\left(\alpha^{(n')} + j\Delta\beta_{jlm}^{(n')}\right)L_f^{(n')}\right)\right], \text{ and} \tag{13}$$

$L_{jlm}^{FWM(n)} = \dfrac{1 - \exp\left(-\left(\alpha^{(n)} + j\Delta\beta_{jlm}^{(n)}\right)L_f^{(n)}\right)}{\alpha^n + j\Delta\beta_{jlm}^{(n)}}$ is the "effective length" of the FWM process

involving frequencies ω_j, ω_l and ω_m in the n-th fiber.

For the special case where all N_s spans are identical and the amplifier gains $G^{(n)} = \exp\left(\alpha^{(n)}L^{(n)}\right)$ exactly equalize the loss of the previous span, (13) can be simplified to:

$$D_{jlm}^{FWM} = \gamma L_{jlm}^{FWM} \exp\left(j\Delta\beta_{jlm}L_f \frac{N_s+1}{2}\right) \frac{\sin\left(\Delta\beta_{jlm}L_f N_s/2\right)}{\sin\left(\Delta\beta_{jlm}L_f/2\right)}. \tag{14}$$

2.1.2 Time-domain approximation

The numerical complexity of evaluating the Volterra series in (9) or (12) is $O\left(M^3\right)$, where M is the total number of spectral components in (4). However, suppose it is possible to define an approximate set of Volterra coefficients $\tilde{D}_{jlm}^{FWM} \approx D_{jlm}^{FWM}$:

$$v{'}_{k}^{(3)}(0) \approx -j \sum_{\substack{j,l,m \\ \in S[k]}} \tilde{D}_{jlm}^{FWM} v_{j}^{(1)} v_{l}^{(1)} \left(v_{m}^{(1)}\right)^{*}, \tag{15}$$

where $v{'}_{m}^{(1)} = W_k(\omega_m)v_m^{(1)}$ is obtained by passing the spectral components $v_m^{(1)}$ through a carefully designed frequency-shaping pre-filter $W_k(\omega_m)$ whose coefficients are such that:

$$W_k\left(\omega_j\right)W_k\left(\omega_l\right)W_k^{*}\left(\omega_m\right) = \tilde{D}_{jlm}^{FWM} \text{ , for } \left(j,l,m\right) \in S[k] \tag{16}$$

It can be shown that:

$$v{'}^{(3)}\left(0,t\right) = \sum_k v{'}_k^{(3)}(0)e^{j\omega_k t} = -j\left|\sum_k v{'}_k^{(1)}e^{j\omega_k t}\right|^{2}\left(\sum_k v{'}_k^{(1)}e^{j\omega_k t}\right) = -j\left|v{'}^{(1)}(t)\right|^{2}v{'}^{(1)}(t), \tag{17}$$

where $v{'}^{(3)}\left(0,t\right) \approx v^{(3)}\left(0,t\right)$ approximates the actual nonlinear perturbation. As according to (16), the filter coefficients are chosen to approximate D_{jlm}^{FWM} at the frequency index k, $v{'}^{(3)}\left(0,t\right) \approx v^{(3)}\left(0,t\right)$ therefore has the highest accuracy around ω_k . The procedure indicated by (17) is as follows:—

1. Multiply the input signal by the pre-filter $v{'}_m^{(1)} = W_k(\omega_m)v_m^{(1)}$.

2. Take the inverse Fourier transform of $v{'}_k^{(1)}$ to obtain $v{'}^{(1)}(t)$.

3. Compute $v{'}^{(3)}(0,t)$ using (17)

4. Take the Fourier transform $v{'}^{(3)}(0,t)$ to obtain the coefficient $v{'}_k^{(3)}$.

5. Repeat steps #1 to #4, using different pre-filters for each frequency index k, until the nonlinear perturbation at all frequency indices are obtained.

Since the fast Fourier transform can be solved efficiently in $O\left(M\log M\right)$ operations, the above procedure has lower numerical complexity $O\left(M^2\log M\right)$ than the corresponding Volterra series in (9) or (12), which have complexity $O\left(M^3\right)$.

It is possible to obtain even greater complexity savings – at the expense of accuracy – if instead of using a different pre-filter each time for #1 to #4, the N frequency indices are partitioned into "subbands" (Weidenfeld et al. 2011). Suppose we modify (16) to:

$$W_b\left(\omega_j\right)W_b\left(\omega_l\right)W_b^{*}\left(\omega_m\right) = \tilde{D}_{jlm}^{FWM} \text{ , for } \left(j,l,m\right) \in \left\{S[k]:\omega_k \in \Omega_b\right\}. \tag{16b}$$

i.e., we design the frequency-shaping $W_b(\omega_j)W_b(\omega_l)W_b^*(\omega_m)$ that approximates D_{jlm}^{FWM} at all frequency indices k where ω_k lies within the subband Ω_b. We invoke the same steps #1 to #3 above replacing W_k with W_b, and for step #4, we use: —

4b. Take the Fourier transform $v'^{(3)}(0,t)$ to obtain the coefficients $v'^{(3)}_k : \omega_k \in \Omega_b$.

In other words, since $v'^{(3)}(0,t)$ has good accuracy around the center frequency of the subband for which W_b was designed, we keep multiple frequency indices at a time. The algorithmic complexity then scales as $O(BM\log M)$, where B is the total number of subbands used.

With $v'^{(3)}(0,t)$ computed, the spectral components of the backpropagated signal can now be found by:

$$u'_k(0) = \left(v_k^{(1)} + \xi v'^{(3)}_k(0)\right)\exp\left(\int_0^L\left(\frac{\alpha(z')}{2} - j\frac{\beta_2(z')\omega_k^2}{2}\right)dz'\right),\tag{18}$$

where $v_k^{(1)} = u_k(L)$. The parameter ξ denotes the overall nonlinear perturbation is scaled, and its value should be optimized for a given launch power level and system dispersion map. It is noted that (18) represents an asymmetric split-step solution, since the nonlinear operator (addition by $v'^{(3)}(0,t)$) is computed first, followed by the linear operator (multiplication by dispersion compensation filter).

2.1.3 Calculating the pre-filter

To find an appropriate frequency-shaping pre-filter, we decompose (16b) into amplitude and phase equations:

$$\log\left|W_b(\omega_j)\right| + \log\left|W_b(\omega_l)\right| + \log\left|W_b(\omega_m)\right| \approx \log\left|D_{jlm}^{FWM}\right|, \text{ and}\tag{19}$$

$$\angle W_b(\omega_j) + \angle W_b(\omega_l) - \angle W_b(\omega_m) \approx \angle D_{jlm}^{FWM},\tag{20}$$

where $(j,l,m) \in \{S[k]:\omega_k \in \Omega_b\}$. These are linear systems of $O(M^3/B)$ equations and M unknowns, and are thus highly over-determined. However, (18) and (19) can be solved via a "best fit" method such as the Moore-Penrose pseudoinverse.[1]

If N is large, the systems of equations may be intractable to solve. Typically, a large N is required when the frequency response $H^+(\omega_k) = \int_0^L -\frac{\alpha(z)}{2} + j\frac{\beta_2(z)}{2}\omega_k^2\,dz$ has large

---

[1] Care should be taken to ensure that the phase of D_{jlm}^{FWM} is properly unwrapped over the indices of interest, before matrix inversion. Note this is a three-dimensional phase-unwrapping procedure.

dispersion over the step size taken. This may be encountered in dispersion-unmanaged transmission for example: if $\varphi_{cd}(\omega) = \beta_2 L \omega^2$ changes rapidly with frequency, the signal must be decomposed with fine spectral resolution in order for each component to remain "frequency-flat" over the step size considered. If (19) and (20) has too many equations to be solved numerically, it is possible to derive the pre-filter heuristically. Consider (14), which gives the Volterra coefficients for a step size equal to N identical fiber spans. Assume the spans are sufficiently long ($L_f \gg 1/\alpha$). Then, it can be shown that for realistic fiber parameters, $L_{jlm}^{FWM} \approx 1/\alpha$ in the neighborhood of $l \approx m \approx k_b$, where k_b is the frequency index of the center of the subband. This neighborhood also contains the strongest components of $D_{jlm}^{FWM} : (j,l,m) \in \{S[k] : \omega_k \in \Omega_b\}$. Hence,

$$\angle D_{jlm}^{FWM} \approx \Delta\beta_{jlm} L_f \frac{N_s + 1}{2} = -\frac{\beta_2}{2} \Delta\omega^2 L_f \left(j^2 + l^2 - m^2 - k^2\right) \frac{N_s + 1}{2}. \tag{21}$$

Noting that phase is quadratic due to dispersion, suppose we choose:

$$\angle W_b(\omega_k) \approx -\frac{\beta_2}{2}(k - k_b)^2 \Delta\omega^2 L_f \frac{N_s + 1}{2}, \tag{22}$$

which centers the quadratic characteristic about ω_{k_b} in the middle of the subband. Similarly for the amplitude equation:

$$\begin{aligned}
\left|D_{jlm}^{FWM}\right| &\approx \frac{\gamma N_s}{\alpha} \frac{1 - \frac{1}{3}\left(\Delta\beta_{jlm} N_s L_f / 2\right)^2}{1 - \frac{1}{3}\left(\Delta\beta_{jlm} L_f / 2\right)^2} \\
&\approx \frac{\gamma N_s}{\alpha} \left[1 - \frac{1}{3}\left(\Delta\beta_{jlm} N_s L_f / 2\right)^2\right]\left[1 - \frac{1}{3}\left(\Delta\beta_{jlm} L_f / 2\right)^2\right] \\
&= \frac{\gamma N_s}{\alpha} \left[1 - \frac{1}{12}\Delta\beta_{jlm}^2\left(N_s^2 - 1\right)L_f^2\right] \\
&\approx \frac{\gamma N_s}{\alpha} \exp\left(-\frac{1}{12}\Delta\beta_{jlm}^2\left(N_s^2 - 1\right)L_f^2\right) \\
&= \frac{\gamma N_s}{\alpha} \exp\left(-\frac{1}{48}\beta_2^2 \Delta\omega^4\left(j^2 + l^2 - m^2 - k^2\right)^2\left(N_s^2 - 1\right)L_f^2\right)
\end{aligned} \tag{23}$$

We thus pick a fourth-order amplitude characteristic about ω_{k_b}:

$$\left|W_b(\omega_k)\right| \approx \left(\frac{\gamma N_s}{\alpha}\right)^{1/3} \exp\left(-\frac{1}{48}\beta_2^2(k - k_b)^4 \Delta\omega^4\left(N_s^2 - 1\right)L_f^2\right). \tag{24}$$

The pre-filter W_b can now be found by combining (22) and (24):

$W_b(\omega) = \left|W_b(\omega)\right| \exp\left(j\angle W_b(\omega)\right).$

2.2 Dual-polarization

For dual-polarization systems, an identical derivation can be carried replacing (3) with the Manakov equation in (2). As before, let $\mathbf{v}_k(z) = \mathbf{u}_k(z)\exp\left(\int_z^L -\left(\frac{\alpha(z')}{2} - j\frac{\beta_2(z')\omega_k^2}{2}\right)dz'\right)$ be the distanced-normalized spectral components of the signal, and let $\mathbf{v}_k(z) = \mathbf{v}_k^{(1)}(z) + \mathbf{v}_k^{(3)}(z)$. It can be shown that the nonlinear perturbation term $\mathbf{v}_k^{(3)}(z) = \left[v_{x,k}^{(3)}(z) \quad v_{y,k}^{(3)}(z)\right]^{\mathrm{T}}$ satisfies:

$$v_{x,k}^2(L) = -j\sum_{\substack{j,l,m \\ \in S[k]}} D_{jlm}^{FWM}\left(v_{x,j}^{(1)}v_{x,l}^{(1)}\left(v_{x,m}^{(1)}\right)^* + v_{x,j}^{(1)}v_{y,l}^{(1)}\left(v_{y,m}^{(1)}\right)^*\right), \text{ and} \tag{25a}$$

$$v_{y,k}^2(L) = -j\sum_{\substack{j,l,m \\ \in S[k]}} D_{jlm}^{FWM}\left(v_{y,j}^{(1)}v_{y,l}^{(1)}\left(v_{y,m}^{(1)}\right)^* + v_{y,j}^{(1)}v_{x,l}^{(1)}\left(v_{x,m}^{(1)}\right)^*\right). \tag{25b}$$

where the Volterra coefficients D_{jlm}^{FWM} are almost identical to those derived for the single-polarization case, with a scaling factor of $(8/9)^{1/3}$ to absorb the factor of $8/9$ in the Manakov equation. Hence for step sizes (i) less than one fiber span, (ii) equal to N_s heterogeneous fibers spans, and (iii) equal to N_s identical fiber spans, D_{jlm}^{FWM} is given by (10), (13) or (14). Thus, the reduced-complexity procedure outlined previously can also be used to find $\mathbf{v}_k^{\prime(3)}(z) \approx \mathbf{v}_k^{(3)}(z)$, with the subband filters given by (19) and (20) using the analytical method, or (22) and (24) using the heuristic method:

$$v_x^{\prime(3)}(0,t) = \sum_k v_{x,k}^{\prime(3)}(0)e^{j\omega_k t} = -j\left(\left|\sum_k v_{x,k}^{\prime(1)}e^{j\omega_k t}\right|^2 + \left|\sum_k v_{y,k}^{\prime(1)}e^{j\omega_k t}\right|^2\right)\left(\sum_k v_{x,k}^{\prime(1)}e^{j\omega_k t}\right), \tag{26a}$$

$$v_y^{\prime(3)}(0,t) = \sum_k v_{y,k}^{\prime(3)}(0)e^{j\omega_k t} = -j\left(\left|\sum_k v_{x,k}^{\prime(1)}e^{j\omega_k t}\right|^2 + \left|\sum_k v_{y,k}^{\prime(1)}e^{j\omega_k t}\right|^2\right)\left(\sum_k v_{y,k}^{\prime(1)}e^{j\omega_k t}\right), \tag{26b}$$

which can be simplified as:

$$\mathbf{v}^{\prime(3)}(0,t) = -j\left|\mathbf{v}^{\prime(1)}(t)\right|^2 \mathbf{v}^{\prime(1)}(t). \tag{27}$$

3. Digital signal processing architecture

The digital signal processing architecture that implements multi-subband, frequency-shaped backpropagation (FS-BP) is shown in Fig. 3(a) (Ip & Bai 2011). It is assumed that a coherent receiver recovers the in-phase (I) and quadrature (Q) components of the electric field in the two signal polarizations, which are synchronously sampled with digital-to-analog

converters (DAC). Shown on the left-hand side of Fig. 3(a) are the received samples $\mathbf{u}(z = L_{tot}, t)\big|_{t=nT}$, where L_{tot} is the total length of the system, and T is the sampling interval. The input signal is processed in block sizes of M samples. For single-carrier (SC) transmission, overlap-and-save is used (Oppenheim & Schafer 2009); for orthogonal frequency-division multiplexing (OFDM) transmission, non-overlapping blocks are taken at the input, with the cyclic prefix of the OFDM symbol (block) stripped at the output. In both cases, the signal processing has the canonical model shown in Fig. 3(a). In the absence of nonlinearity, the operations enclosed between the fast Fourier transform (FFT) and inverse FFT (IFFT) performs frequency-domain linear equalization (LE) of chromatic dispersion. In digital backpropagation, the single "linear step" is replaced with a concatenation of nonlinear and linear steps, as outlined in Section 2.

Fig. 3(b) shows a generalized model of the nonlinear step. The input signal is multiplied by the pre-filter derived in Section 2. To avoid aliasing, we upsample the input signal by padding with zeros in the frequency domain, before taking a $2M$–point inverse FFT (IFFT). The nonlinear perturbation is then computed in the time-domain. After taking a $2M$–point FFT to recover the frequency components, we downsample by stripping the high-frequency components, followed by multiplication by a "post-filter." These operations are repeated for the B subbands. Summing their outputs yield an overall nonlinear perturbation, which is then scaled and summed with the through signal.
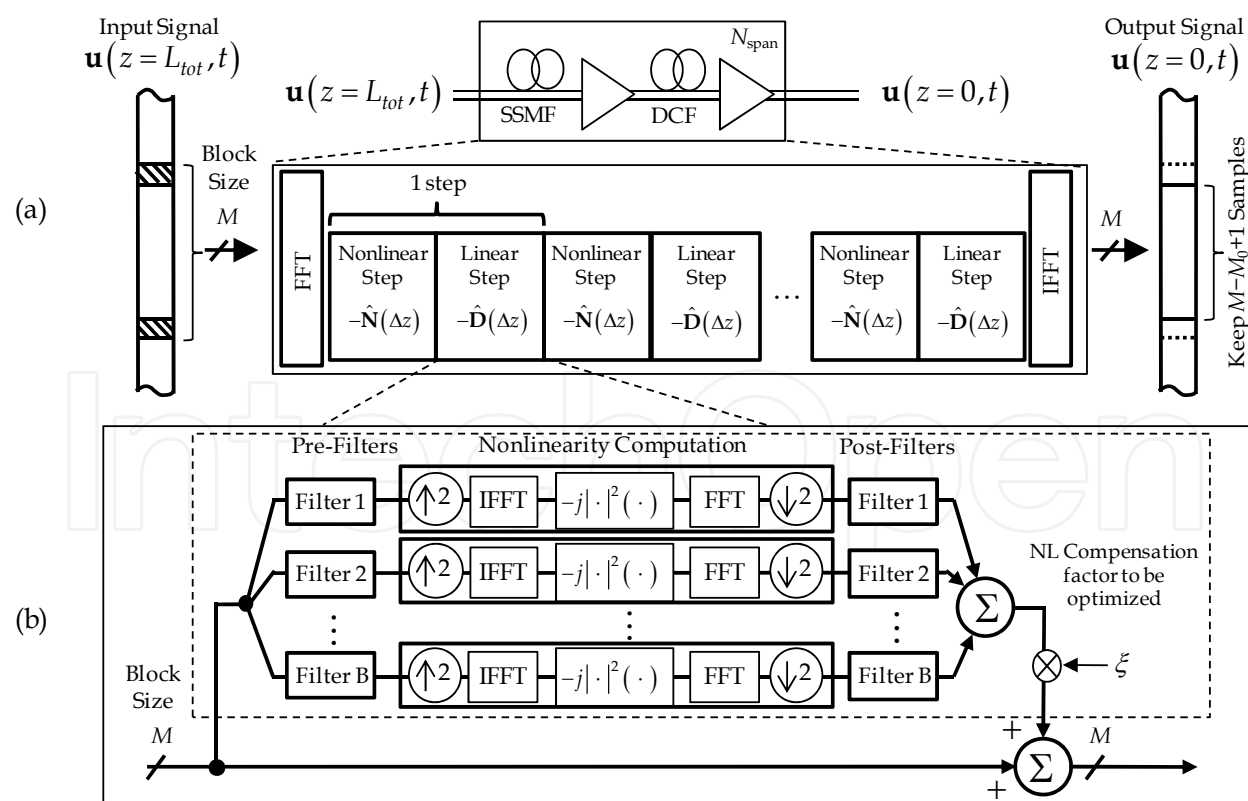

Fig. 3. (a) Digital Backpropagation using overlap-and-save, (b) Enhanced nonlinearity computation using subbanding and frequency shaping by pre- and post-filters.

Note that we have not discussed a method of calculating the post-filter. In Section 2, it was assumed that after computing $\mathbf{v'}_k^{(3)}$ in (17) or (27), we keep only the spectral components $\{k : \omega_k \in \Omega_b\}$ in the neighborhood of ω_{k_b}. This corresponds to multiplying $\mathbf{v'}_k^{(3)}$ by a rectangular filter whose support spans the bandwidth Ω_b. It is possible to use other filter shapes for the post-filters, which may have better performance than simple rectangular filters. However, this is not covered by the current work.

Algorithmic complexity can be determined directly from Fig. 3(b). Assume the use of overlap-and-save in Fig. 3(a) where adjacent blocks overlap by M_0 samples. We assume a K steps in the backpropagation, and that the post-filters are rectangular filters (no multiplications required). It can be shown that the complexity for FS-BP for single-polarization signals is:

$$C_{FS-BP,1pol} = \left(\left[\left(4(2M)\log_2(2M) + 12M \right)B + 4M \right]K + 4M\log_2 M \right) \big/ \left(M - M_0 + 1 \right). \quad (28)$$

For dual-polarization signals, the complexity of FS-BP is:

$$C_{FS-BP,2pol} = \left(\left[\left(8(2M)\log_2(2M) + 24M \right)B + 8M \right]K + 8M\log_2 M \right) \big/ \left(M - M_0 + 1 \right). \quad (29)$$

We note that standard backpropagation is merely a special case of FS-BP where the nonlinearity perturbation is computed without pre- and post-filters (frequency-flat), and only $B = 1$ subband is used. Hence the complexity of standard backpropagation (Std.BP) for single- and dual-polarization signals are:

$$C_{Std.BP,1pol} = \left(\left[4(2M)\log_2(2M) + 8M \right]K + 4M\log_2 M \right) \big/ \left(M - M_0 + 1 \right) \text{, and} \quad (30)$$

$$C_{Std.BP,2pol} = \left(\left[8(2M)\log_2(2M) + 16M \right]K + 8M\log_2 M \right) \big/ \left(M - M_0 + 1 \right). \quad (31)$$

Finally, for linear equalization (LE), the complexities for single- and dual-polarization signals are:

$$C_{LE,1pol} = \left(4M + 4M\log_2 M \right) \big/ \left(M - M_0 + 1 \right) \text{, and} \quad (32)$$

$$C_{LE,2pol} = \left(8M + 8M\log_2 M \right) \big/ \left(M - M_0 + 1 \right). \quad (33)$$

The motivation for the use of sub-banding, pre-filtering and post-filtering can be understood as follows: in a dispersive fiber, different frequency components of a signal propagate at different speeds. From the point of view of a particular frequency component, the other frequencies walk off. Walk-off has an averaging effect on their mutual nonlinear interaction. Hence, a frequency component of interest experiences stronger nonlinear effects from frequencies closer to it than frequencies further away. To compute nonlinear perturbation at a particular frequency ω_{k_b}, therefore, one should weight the input signal with a pre-filter that emphasizes the frequencies close to it, while suppressing frequencies farther away (Fig. 4). The nonlinearity computed using this method will be accurate around ω_{k_b}. To compute nonlinearity accurately around other frequencies, different pre- and post-filters are needed.
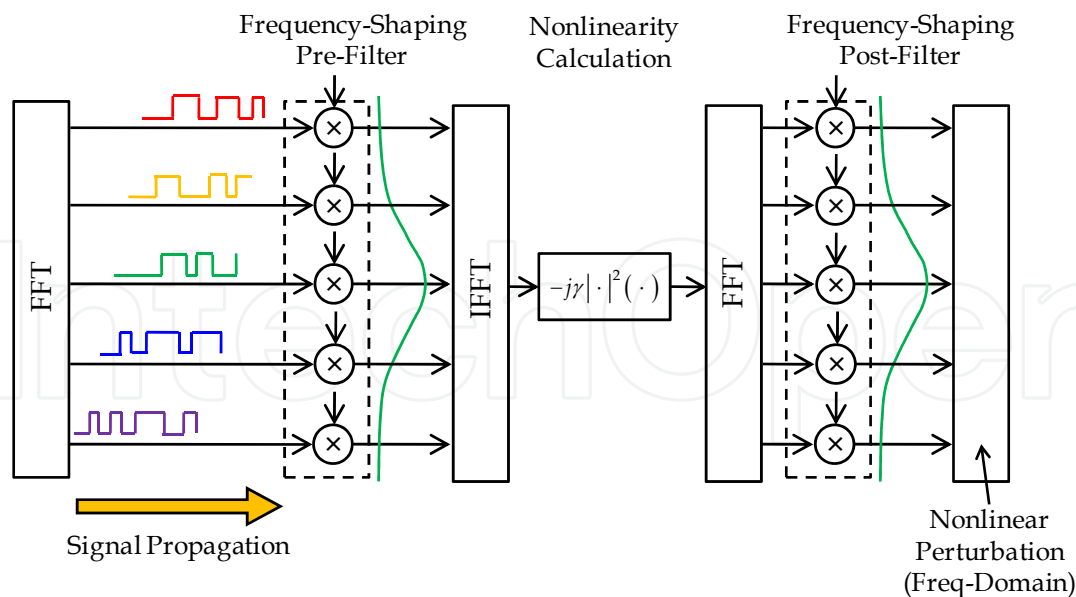
Fig. 4. Physical interpretation of enhanced nonlinearity computation.

4. Results

In this section, we will investigate the efficacy of FS-BP by numerical simulation for two systems (Fig. 5):—

a. OFDM transmission over 12×80-km spans of single-mode fiber (SSMF) (Attenuation = 0.2 dB/km, Dispersion = 17 ps/nm/km and Nonlinear parameter 0.0013 W^{-1}), with full dispersion management after each span using dispersion compensation fiber (DCF) (Attenuation = 0.5 dB/km, Dispersion = −85 ps/nm/km and Nonlinear parameter 0.0053 W^{-1}). The launch power into DCF is assumed to be 6 dB lower than that into SSMF. For the signal, 112-Gb/s OFDM is assumed. The total number of subcarriers (FFT size) is 128. Of these, 102 are modulated with dual-polarization 16-QAM (DP-QAM). A cyclic prefix of 20 is appended for each block.

b. SC transmission over 24×80-km spans of low-dispersion fiber (Attenuation = 0.2 dB/km, Dispersion = 2 ps/nm/km and Nonlinear parameter 0.0013 W^{-1}), with no inline dispersion management. The signal is assumed to be 112-Gb/s DP-16QAM.

For both systems and for all algorithms to be compared, it is assumed that the received signal $\mathbf{u}(L,t)$ is oversampled by a factor of two relative to the chip rate. i.e., For System A, $T = 1/[(112\times10^9/8)\times((128+20)/102)\times2] = 24.6$ ps; for System B, $T = 1/[(112\times10^9/8)\times2] = 35.7$ ps. Overlap-and-save is assumed (Fig. 3(a)). The block size used varies depending on the amount of dispersion to be compensated per step, but the smallest power-of-two is chosen subject to the condition that there be minimal loss of performance due to frequency discretization.

Fig. 6 shows the amplitude and phase of the Volterra coefficients D_{jlm}^{FWM} for System A at DC ($k = 0$), assuming a step size equal to four spans (i.e., $K = 3$ steps for the entire link). As expected, the largest coefficients are found around $l = 0$ and $m = 0$, as the corresponding frequencies ω_l and ω_m are closest to ω_k of interest, therefore contributing to the most nonlinear effects.
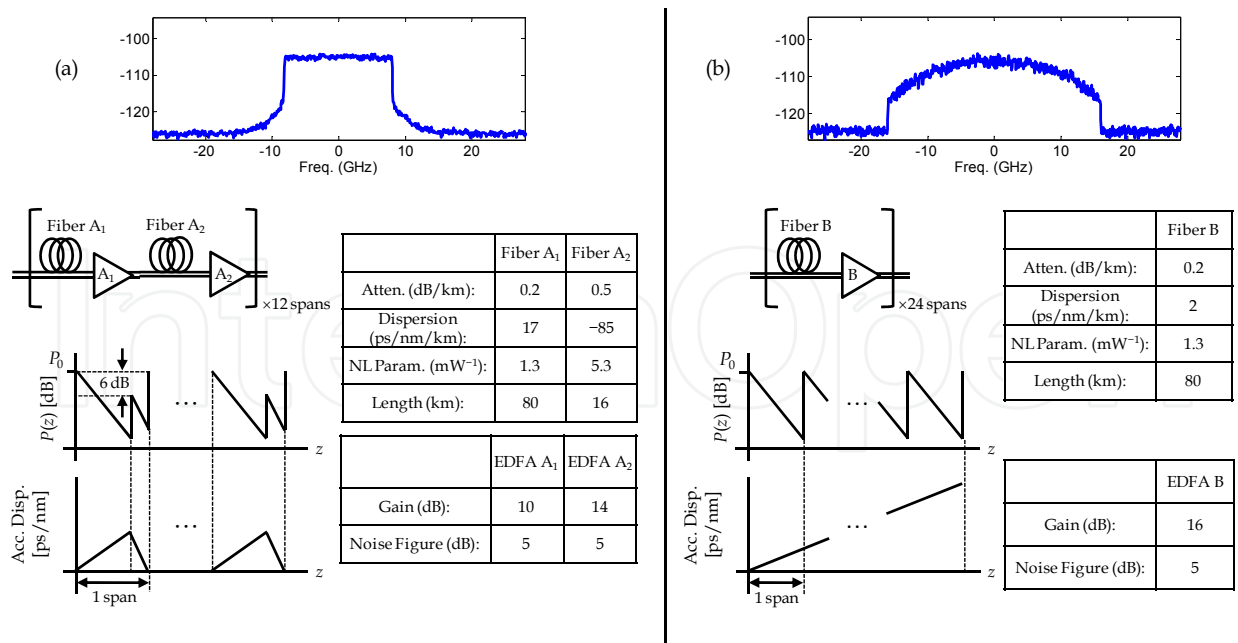
Fig. 5. Simulation setup for (a) System A and (b) System B, showing the signal spectrum, dispersion map, power profile, and fiber & EDFA parameters.
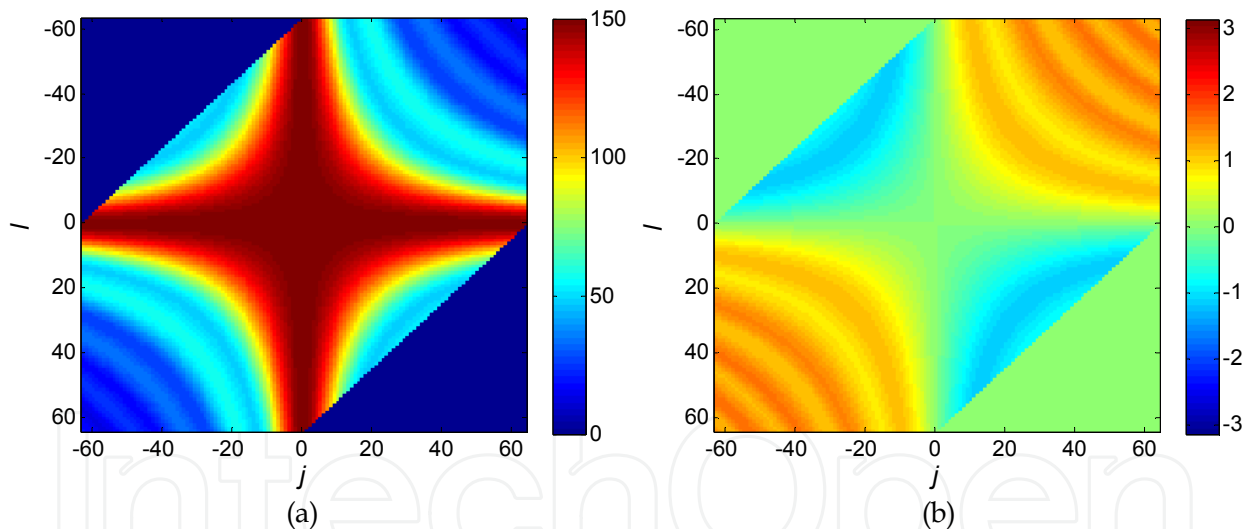

Fig. 6. (a) Amplitude and (b) Phase of D_{jlm}^{FWM} at $k=0$ for System A.

We assume that a block size of $M=128$ is used, and the signal is partitioned into $B=3$ subbands of equal bandwidth. Using (13), (19), and (20), the pre-filter for each subband is computed, and their amplitude and phase responses are shown in Fig. 7. Subband filter #1 is used to compute the nonlinear perturbation at the lowest frequencies (frequency indices $-64 \le k \le -22$); subband filter #2 is use for the frequencies near DC ($-21 \le k \le 21$), and subband filter #3 for the highest frequencies ($22 \le k \le 63$). As expected, the amplitude response of each subband filter has a maximum at the center of each subband. In addition, the phases of the pre-filters are approximately quadratic, accounting for the effect of fiber dispersion.

(a)   (b)
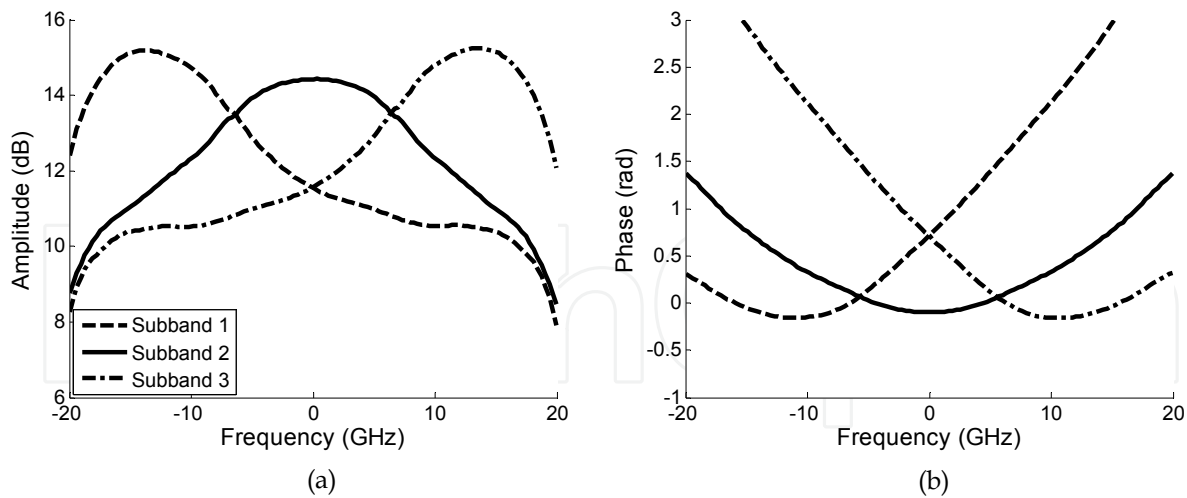
Fig. 7. (a) Amplitude and (b) Phase responses of subband pre-filters for System A.

To see how well the FS-BP technique emulates the actual Volterra coefficients, we evaluate $\tilde{D}_{jlm}^{FWM} = W_k(j)W_k(l)W_k^*(m)$ at $k = 0$, since these are the "approximate" Volterra coefficients that will result from the application of (17). Fig. 8 shows the amplitude and phase of $\tilde{D}_{jlm}^{FWM}$ at $k = 0$. Compared with Fig. 6, we observe good match between the amplitude and phase of D_{jlm}^{FWM} and $\tilde{D}_{jlm}^{FWM}$ around $l = m = 0$ where most of the energy is located. This indicates the effectiveness of FS-BP to mimic the $O(M^3)$ complexity Volterra series.

(a)   (b)
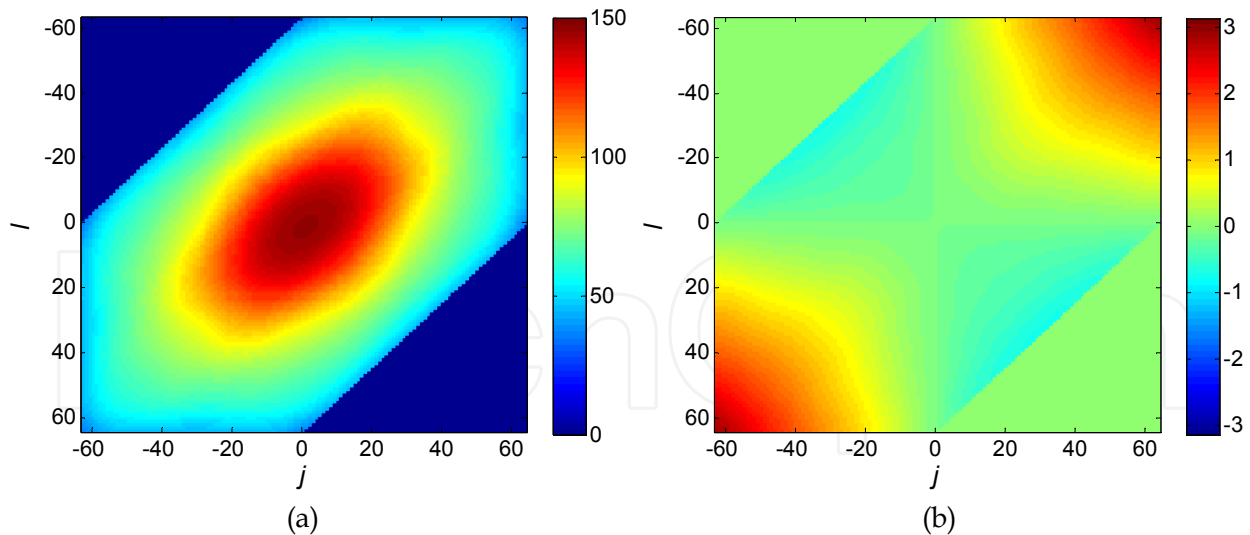
Fig. 8. (a) Amplitude and (b) Phase of $\tilde{D}_{jlm}^{FWM}$ at $k = 0$ for System A.

We repeated the results for System B in Figs. 7−9. The block size and number of subband are again assumed to be $M = 128$ and $B = 3$, and the step size is set to four spans (i.e., $K = 6$ for the entire link). The amplitude and phase of the actual Volterra coefficients D_{jlm}^{FWM} at $k = 0$ are shown in Fig. 9. We use the "heuristic" model (22) and (24) to compute the pre- filters.
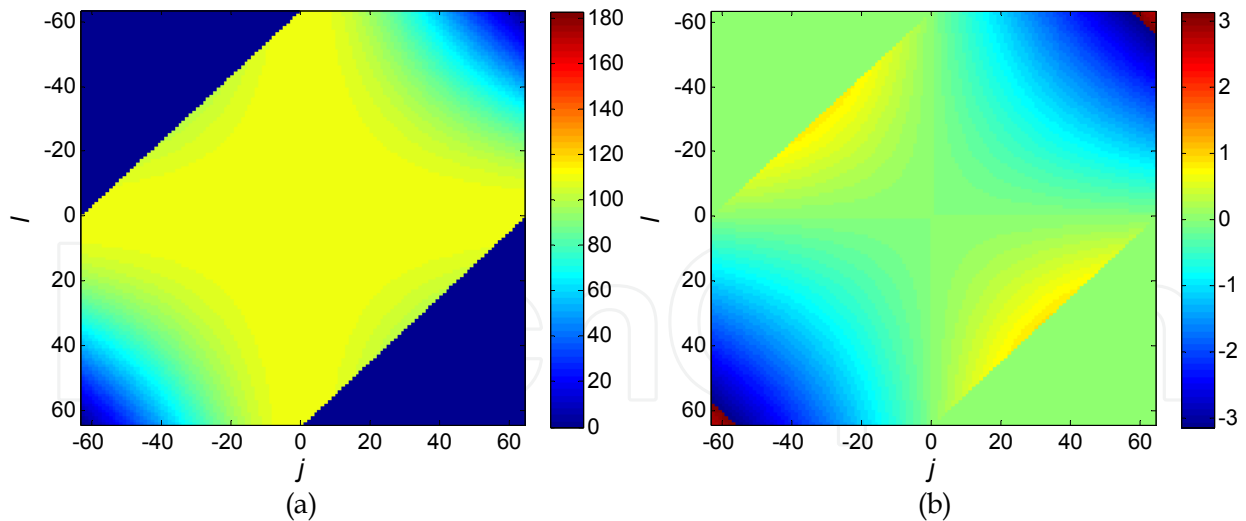
Fig. 9. (a) Amplitude and (b) Phase of D_{jlm}^{FWM} at $k = 0$ for System B.

The phase and amplitude responses of the pre- filters are shown in Fig. 10, with their corresponding $\tilde{D}_{jlm}^{FWM}$ at $k = 0$ shown in Fig. 11. While excellent match between the phases of Fig. 9(b) and Fig. 11(b) is observed, the amplitudes in Fig. 11(a) of the "approximate" Volterra coefficients are larger than the actual Volterra coefficients. Thus, using the pre-filters in Fig. 10 will overestimate the nonlinearity perturbation at each step. In the nonlinearity computation block shown in Fig. 3(b) (also equation (18)), ξ will need to be adjusted to optimize system performance for each power level.

To see how much FS-BP improves system performance across the frequencies, Fig. 12 compares FS-BP with LE for System A, assuming a launch power of $P_0 = -2$ dBm. We use the notation FS-BP[K:B] to denote that K backpropagation steps are used, and in each step, the signal is partitioned into B equal subbands for nonlinearity computation. We evaluate system performance by the Q-factor, which is defined as the mean signal power divided by the mean signal distortion after compensation, i.e., Q is the inverse of error vector
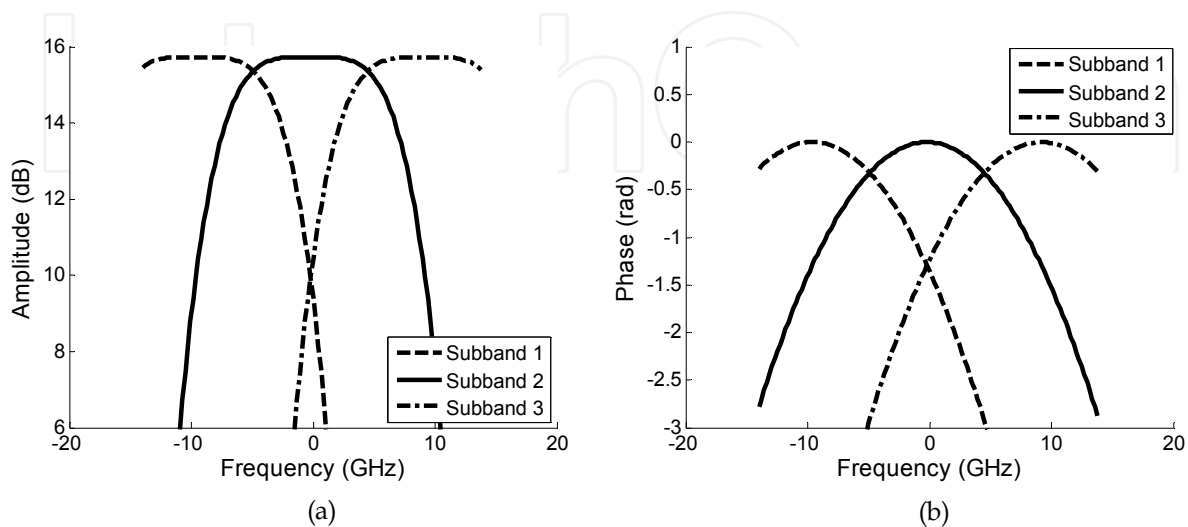

Fig. 10. (a) Amplitude and (b) Phase responses of subband pre-filters for System B.
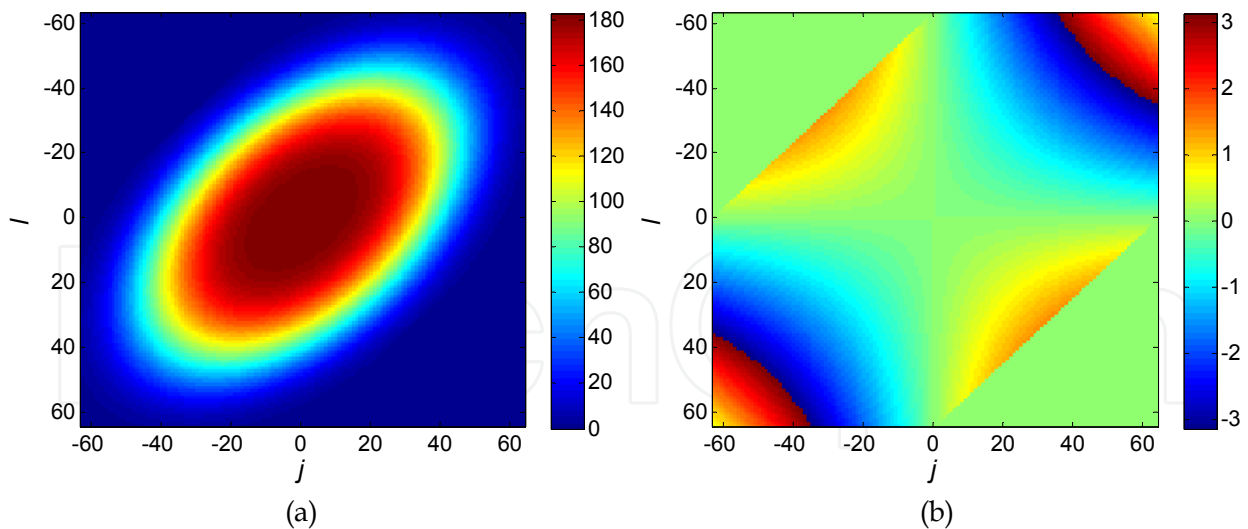
(a)   (b)

Fig. 11. (a) Amplitude and (b) Phase of $\tilde{D}_{jlm}^{FWM}$ at $k = 0$ for System B.
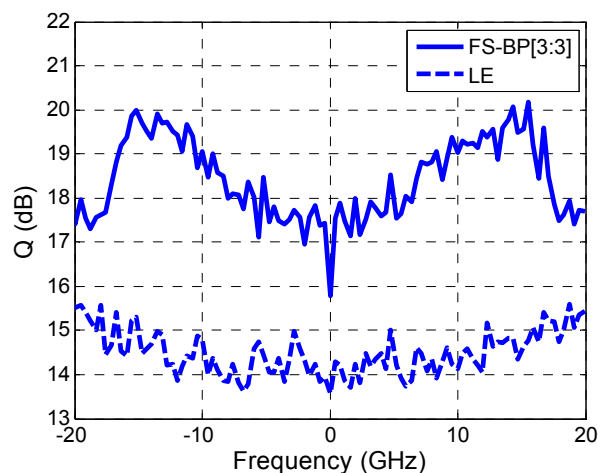

Fig. 12. Q vs. Frequency for System A, comparing different impairment compensation algorithms.

magnitude (EVM). For both LE and FS-BP, it is observed that the outer subcarriers have higher Q than the inner subcarriers, due to reduced number of neighboring subcarriers carrying data contributing to nonlinearity. The use of FS-BP improves the performance for all of the subcarriers. However, the improvement is not uniform. It is observed that the subcarriers around ±15 GHz have the best performance because they correspond to the center of subbands 1 and 3, about which the pre-filters #1 and #3 were optimized.

Next, we investigate system performance versus launch power, and how algorithmic complexity trades off with system performance. We compare (i) linear equalization only (LE), (ii) FS-BP, and (iii) standard backpropagation (Std. BP) with one or more steps per fiber span.

Figs. 13 and 14 show the results for System A and System B. In Figs. 11(a) and 12(a), it is observed that as the number subbands and/or BP sections used is increased, system performance improves as expected. Standard BP with one step per span outperforms the FS-BP algorithms with multi-span step sizes, but has significantly higher algorithmic
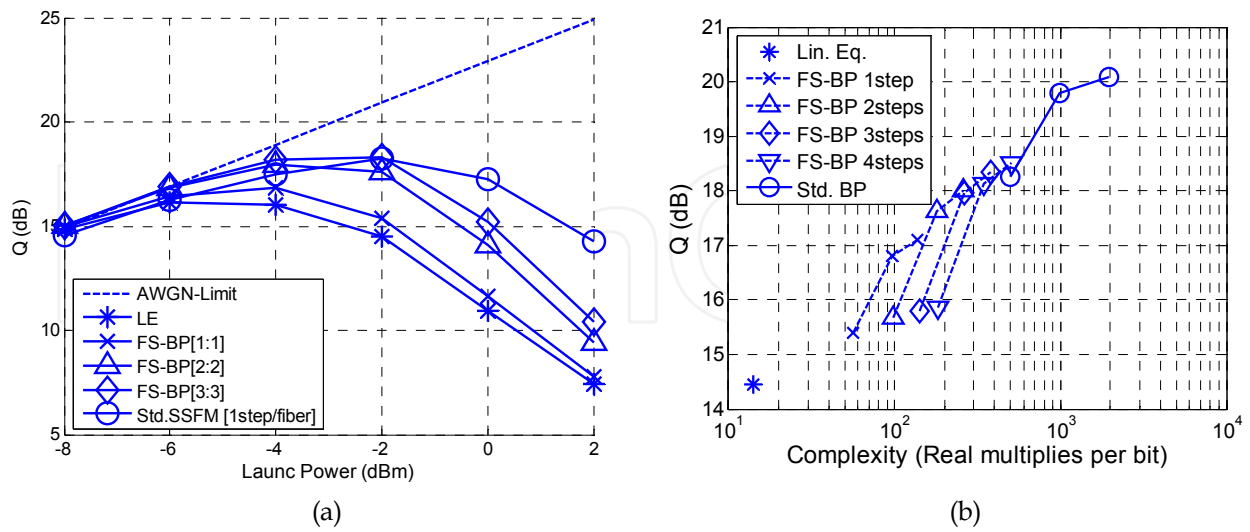
Fig. 13. (a) Performance vs. Launch Power (b) Performance vs. Complexity for System A, comparing different impairment compensation algorithms.
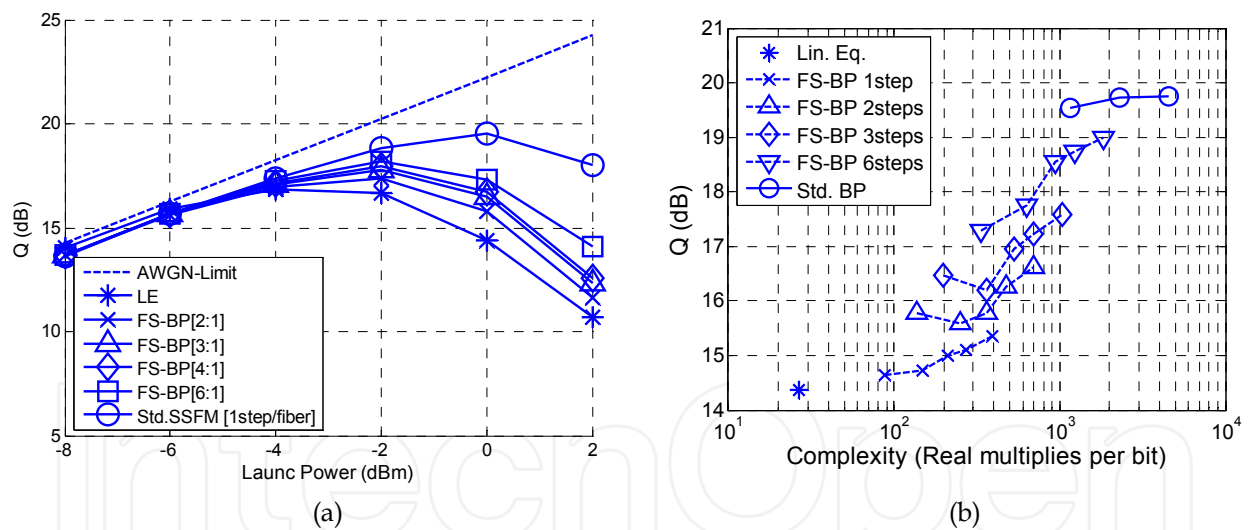

Fig. 14. (a) Performance vs. Launch Power (b) Performance vs. Complexity for System B, comparing different impairment compensation algorithms.

complexity. Figs. 11(b) and 12(b), shows Q versus algorithmic complexity as defined by (28)−(33). The curves labeled "FS-BP K steps" denotes using FS-BP with K DBP steps and varying number of subbands. As the number of subbands is increased from left to right, complexity increases and performance improves. The curve labeled Std. BP denotes standard DBP (frequency-flat) with varying number of steps per span. As the total number of steps increases from left to right, complexity increases and performance improves. Both Systems A and B confirm the performance vs. complexity tradeoff, but they differ on the

optimal nonlinearity compensation strategy for a given complexity. For System A, it is observed that for a given complexity, better performance is obtained using fewer steps and more subbands. Conversely, for System B, it is better to employ more steps, but to use only one subband for nonlinearity calculation at each step. This result is intuitively meaningful. In dispersion managed transmission, the signal will have the same amplitude profile after every span (except for noise and nonlinearity, which are small). Hence, dividing the link into larger number of steps will have little performance improvement. By contrast, dividing the signal into subbands will improve the accuracy of the nonlinearity computation, hence better performance. In dispersion unmanaged transmission, the signal profile change rapidly after each step. It is therefore better to use larger number of steps, with strong filtering of the nonlinear perturbation since these will experience strong averaging effect with dispersion. Fig. 10(a) (and equation (24)) confirmed the second-order Gaussian steepness of the amplitude pre-filter. The small dip in Q in Fig. 14(b) at two subbands for FS-BP with 2 and 3 steps is due to the nature of single-carrier signals, where frequencies near DC are the most important. When using one subband, nonlinearity is well compensated near DC, but when using two subbands, the center of the subbands will straddle DC, so nonlinearity is slightly less-well compensated at the most critical frequency.

Finally, Figs. 13(b) and 14(b) indicates that by selecting an optimal number of steps and subbands, FS-BP can provide around 2.5 dB improvement over LE at ten times the algorithmic complexity for both Systems A and B, which is significant savings compared with frequency-flat BP at one step per span. This may make FS-BP an attractive candidate for real-time implementation.

5. Conclusions

In dispersive optical fiber, a given frequency component of a signal experiences stronger nonlinear interactions from frequencies closer to it than frequencies far away. This walkoff effect can be exploited by multiplying the signal with a set of pre-filters, each designed to enable nonlinear perturbation be calculated accurately around a design frequency. By combining the different estimates together, nonlinear perturbation can be calculated accurately across the entire signal bandwidth, allowing backpropagation to use larger step sizes. This muti-subband frequency-shaped backpropagation (FS-BP) approach allows flexible tradeoff between performance and complexity as the number of steps and the number of subbands can be independently varied. We simulated FS-BP for two systems: OFDM transmission over a dispersion-managed link, and single-carrier transmission over a dispersion-unmanaged link. It was found that a dispersion-managed link favors using fewer steps but larger number of subbands; whereas a dispersion-unmanaged link favors using more steps at one subband per step. For both systems, it was found that FS-BP can improve system performance by as much as 2.5 dB at a computational cost ten times that of linear equalization only. This makes FS-BP a potentially candidate for real-time implementation where low algorithmic complexity is essential.

6. References

Agrawal, G. P. (2001). *Nonlinear Fiber Optics 3rd Edition*, Academic Press, ISBN 0120451433, San Diego, CA, U.S.A.

Du, L. B. & Lowery, A. J. (2010). Improved single channel backpropagation for intra-channel fiber nonlinearity compensation in long-haul optical communications systems, *Optics Express*. Vol. 18, No. 16, (August 2010), pp. 17075−17088, ISSN 1094-4087.

Essiambre, R.-J.; Foschini, G. J.; Winzer, P. J.; Kramer, G. & Burrows, E. C. (2008). The capacity of fiber-optic communication systems, *Proceedings of the Optical Fiber Communications Conference (OFC 2008)*, Paper OTuE1, San Diego, CA, U.S.A., March 2008.

Ip, E. & Kahn, J. M. (2010). Fiber impairment compensation using coherent detection and digital signal processing, *Journal of Lightwave Technology*, Vol. 28 No. 4, (February 2010) pp. 502−519, ISSN 0733-8724.

Ip, E. & Kahn, J. M. (2008). Compensation of dispersion and nonlinear impairments using digital backpropagation, *Journal of Lightwave Technology*, Vol. 26, No. 20, (October 2008) pp. 3416−3425, ISSN 0733-8724.

Ip, E. & Bai, N. (2011). The Nonlinear compensation using frequency-shaped multi-subband backpropagation, *Proceedings of the Optical Fiber Communications Conference (OFC 2011)*, Paper OThF4, Los Angeles, CA, U.S.A., March 2011.

Li, L.; Tao, Z.; Dou, L.; Yan, W.; Oda, S.; Tanimura, T.; Hoshida, T. & Rasmussen, J. (2011). Implementation efficient nonlinear equalizer based on correlated digital backpropagation, *Proceedings of the Optical Fiber Communications Conference (OFC 2011)*, Paper OWW3, Los Angeles, CA, U.S.A., March 2011.

Li, X.; Chen, G.; Goldfarb, G.; Mateo, E.; Kim, I.; Yaman, F. & Li, G. (2008). Electronic post-compensation of WDM transmission impairments using coherent detection and digital signal processing, *Optics Express*. Vol. 16, No. 2, (January 2008), pp. 880−888, ISSN 1094-4087.

Marcuse, D., Menyuk, C. R. & Wai, P. K. A. (1997). Applications of the Manakov-PMD equation to studies of signal propagation in optical fibers with randomly varying birefringence, *Journal of Lightwave Technology*, Vol. 15, No. 9, (September 1997) pp. 1735−1746, ISSN 0733-8724.

Nazarathy, M.; Khurgin, J.; Weidenfeld, R.; Meiman, Y.; Cho, P.; Noé, R., Shpantzer, I. & Karagodsky, V. (2008). Phased-array cancellation of nonlinear FWM in coherent OFDM dispersive multi-span links, *Optics Express*. Vol. 16, No. 20, (September 2008), pp. 15777−15810, ISSN 1094-4087.

Oppenheim, A. V. & Schafer, R. W. (2009). *Discrete-Time Signal Processing 3rd Edition*, Prentice Hall, ISBN 0131988425, Upper Saddle River, NJ, U.S.A.

Sinkin, O. V.; Holzlöhner, R.; Zweck, J. & Menyuk, C. (2003). Optimization of the split-step Fourier method in modelling optical-fiber communication systems, *Journal of Lightwave Technology*, Vol. 21, No. 1, (January 2003) pp. 61−68, ISSN 0733-8724.

Weidenfeld, R.; Nazarathy, M.; Noé, R. & Shpantzer, I. (2010). Volterra nonlinear compensation of 100G coherent OFDM with baud-rate ADC, tolerable complexity and low intra-channel FWM/XPM error propagation, *Proceedings of the Optical Fiber Communications Conference (OFC 2010)*, Paper OTuE3, Los Angeles, CA, U.S.A., March 2011.

Zhang, Q. & Hayee, M. I. (2008). Symmetrized split-step Fourier scheme to control global simulation accuracy in fiber-optic communication systems, *Journal of Lightwave Technology*, Vol. 26, No. 2, (January 2008) pp. 302−316, ISSN 0733-8724.
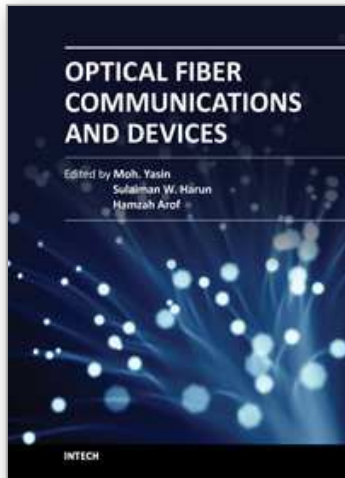
Optical Fiber Communications and Devices

Edited by Dr Moh. Yasin

This book is a collection of works dealing with the important technologies and mathematical concepts behind today's optical fiber communications and devices. It features 17 selected topics such as architecture and topologies of optical networks, secure optical communication, PONs, LANs, and WANs and thus provides an overall view of current research trends and technology on these topics. The book compiles worldwide contributions from many prominent universities and research centers, bringing together leading academics and scientists in the field of photonics and optical communications. This compendium is an invaluable reference edited by three scientists with a wide knowledge of the field and the community. Researchers and practitioners working in photonics and optical communications will find this book a valuable resource.

How to reference

In order to correctly reference this scholarly work, feel free to copy and paste the following:

Ezra Ip and Neng Bai (2012). Nonlinear Compensation Using Multi-Subband Frequency-Shaped Digital Backpropagation, Optical Fiber Communications and Devices, Dr Moh. Yasin (Ed.), ISBN: 978-953-307-954-7, InTech, Available from: http://www.intechopen.com/books/optical-fiber-communications-and-devices/nonlinear-compensation-using-multi-subband-frequency-shaped-digital-backpropagation

INTECH

open science | open minds